Neutral transport analysis of recent DIII-D neutral density experiments



2003 Nucl. Fusion 43 314

(http://iopscience.iop.org/0029-5515/43/5/303)

INSTITUTE OF PHYSICS PUBLISHING and INTERNATIONAL ATOMIC ENERGY AGENCY NUCLEAR FUSION

Nucl. Fusion **43** (2003) 314–320 PII: S0029-5515(03)61219-6

# Neutral transport analysis of recent DIII-D neutral density experiments

**J. Mandrekas**[1], **R.J. Colchin**[2], **W.M. Stacey**[1], **D. Zhang**[1] **and L.W. Owen**[2]

[1] Georgia Institute of Technology
[2] Oak Ridge National Laboratory

Received 16 July 2002, accepted for publication 19 March 2003
Published 15 April 2003
Online at stacks.iop.org/NF/43/314

**Abstract**
Recent measurements of the neutral densities both inside and outside the separatrix near the $X$-point of the DIII-D tokamak, in both L- and H-mode plasmas, are analysed with the two-dimensional transmission/escape probability neutral transport code GTNEUT and with the two-dimensional Monte Carlo code DEGAS. The predictions of the two codes are in good agreement with each other and agree with the experiment to within the experimental error bars in most cases.

**PACS numbers:** 52.25.Ya, 52.70.Nc

## 1. Introduction

The neutral density at the edge near the $X$-point of the DIII-D tokamak has been recently measured in both L-mode and H-mode discharges. The novel experimental method employed [1] consisted of measuring the $D_\alpha$ light emission in the lower divertor by means of a tangentially viewing charge injection device (CID) video camera (TTV) [2].

The availability of such measurements offers us a unique opportunity to compare the predictions of neutral transport codes with experiment. Such a direct comparison between computation and experiment is not very common, since reliable measurements of the neutral densities at the edge of present-day fusion devices are relatively scarce. The purpose of this paper is to compare the predictions of the two-dimensional neutral transport code GTNEUT and the two-dimensional Monte Carlo code DEGAS [3] with the recent DIII-D measurements and with each other. The GTNEUT code is based on the transmission/escape probabilities (TEP) methodology [4] and it has been benchmarked extensively against Monte Carlo codes [5, 6].

Previous calculations of the L-mode DIII-D experiment have shown the potential of the TEP method to predict neutral densities in realistic experimental geometries. A calculation of the L-mode experiment in DIII-D [1] using a simplified, few region TEP model yielded reasonable agreement with the data and with the DEGAS predictions [7]. Subsequent simulations of the same L-mode experiment using the full GTNEUT code also showed relatively good agreement between GTNEUT and the experiment, as well as with the Monte Carlo code DEGAS [6]. However, these comparisons also highlighted several limitations in the physics models in the original GTNEUT code, the most important of which was the lack of a realistic wall reflection model.

In this paper, an upgraded version of the GTNEUT code with a realistic reflection model, a 'two-group' treatment of the neutral energy dependence and the ability to use the same cross-section libraries used in the DEGAS code is used [8]. The original L-mode experiment is revisited and, in addition, a more recent H-mode experiment is described and analysed. Predictions based on the Monte Carlo code DEGAS are also included for both cases.

This paper is organized as follows: in section 2, the L- and H-mode experiments are described. The GTNEUT code, including the recent upgrades, is briefly described in section 3. The results of our simulations and comparisons with experiment and Monte Carlo are presented in section 4. Finally, summary and conclusions follow.

## 2. Experimental determination of divertor neutral densities

When plasma recycles in the divertor, both atoms and molecules are produced and transported into the plasma. With electron temperatures of $\geqslant 10$ eV, neutral molecules entering the divertor scrape off layer (SOL) are initially broken up within a short distance ($\sim 1$ cm) either by molecular dissociation or dissociative ionization [9]. The former process produces the so-called 'Frank-Condon' neutral atoms with an energy of a few electronvolts, which can penetrate through the SOL and into the plasma edge. Electron impact excitation of these atoms produces a $D_\alpha$ radiating volume much larger than that of the molecular source. Charge exchange with fast

  

plasma ions further enlarges this volume. We have employed the $D_\alpha$ light in this volume to measure the density of neutral particles.

Neutral densities have been measured in the divertor of DIII-D by the technique described in [1]. $D_\alpha$ light is recorded by a tangentially-viewing TV camera [2] which views the lower divertor region in DIII-D. This light is inverted using a matrix inversion technique to construct a map of the $D_\alpha$ light intensity in a poloidal plane. Restrictions in the data inversion and the intensity resolution of the camera at the $X$-point limit the resolution of the data to blocks of $6 \times 2\,\mathrm{cm}^2$ (W × H), although the diagnostic is capable of $2 \times 2\,\mathrm{cm}^2$ resolution. Simultaneous $D_\alpha$ and $D_\beta$ measurements made using calibrated photomultipliers are used to calibrate the inverted light intensity of the tangential TV camera. Neutral densities are determined from the calibrated $D_\alpha$ data by assuming that the light arises from electron excitation of neutral atoms according to the relation $I_{D_\alpha} = n_e n_0 \langle \sigma(T_e, n_e) v_e \rangle_{exc}$ where $I_{D_\alpha}$ is the intensity from the tangential TV, $\langle \sigma(T_e, n_e) v_e \rangle_{exc}$ is the electron rate coefficient obtained from a collisional radiative (CR) model [10, 11], $n_0$ is the neutral density, and $n_e$ is the electron density. According to the CR model, the excited state distribution of the atoms is determined by a balance between collisional (including de-excitation, as well as excitation) and radiative processes. It should be emphasized that the key to this technique is the availability of local divertor Thomson measurements of the electron densities and temperatures $n_e$ and $T_e$, at the points where $n_0$ is to be evaluated [12, 13].

Divertor neutral densities were measured in both L-mode and quiescent H-mode plasmas. For the discharges analysed, the plasma current was 1.0 MA and the magnetic field was 2.1 T. The line averaged densities were $n_e = 2.4 \times 10^{19}\,\mathrm{m}^{-3}$ in the L-mode and $n_e = (4.1\text{–}6.2) \times 10^{19}\,\mathrm{m}^{-3}$ at different times in the H-mode. Results are plotted in figure 1, as a function of $1 - \Psi$, where $\Psi$ is the normalized flux. The abscissa is chosen to be $1 - \Psi$ because the $X$-point height was varied between measurements and because the large flux expansion near the $X$-point causes the variation in $\Psi$ values to be very small. The $X$-point is marked by a vertical line at $1 - \Psi = 0$.

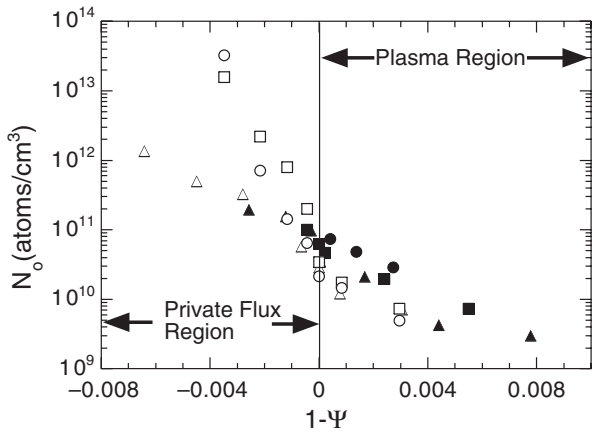


**Figure 1.** Neutral densities as a function of $1 - \Psi$, where $\Psi$ is the normalized flux. Open symbols denote L-mode data (shot 96740) and closed symbols H-mode data. $X$-point heights above the divertor floor: △—11 cm, □—7.2 cm, ○—3.6 cm. Data from shots 96740 and 96747.

In figure 1, the H-mode neutral densities are plotted as solid symbols, and lie slightly above the L-mode points (open symbols) inside the $X$-point. Similar behaviour has been observed at the midplane, on edge flux surfaces. Note in figure 1 that as the extent of the private flux region was reduced by lowering the $X$-point closer to the divertor floor (open circles and squares), the neutral density dependence on $1 - \Psi$ in the private flux region was compressed toward the $X$-point.

The excitation rate coefficients are very sensitive functions of the local electron temperature at low values of $T_e$ ($T_e < 2\,\mathrm{eV}$). For that reason, neutral densities are only measured at the locations of divertor Thomson scattering points. Photon statistics coupled with the sensitivity of the excitation rate cross-sections at low $T_e$ values lead to large error bars in the cool plasma located in the private flux region between the $X$-point and the divertor floor.

In addition to errors due to photon scattering, data errors also arise from inversion of the tangential TV $D_\alpha$ light. The data are smoothed using a least-squares fitting routine and the (asymmetric) residuals are used in error calculations. Data errors also arise from an indeterminacy of the exact value of the camera's zero light level. Erroneous neutral densities will be determined if $D_\alpha$ photons result from recombination rather than excitation. For the discharges analysed, $D_\alpha / D_\beta$ ratios of 13–15 indicate that there is no recombination in the lines of sight of the calibrating photomultipliers.

$D_\alpha$ photons may also be emitted following dissociative processes involving $D_2$ or $D_2^+$ that lead to excited atoms. These emissions should not constitute a large source of error for the analysis of atomic densities except near recycling sites or in regions of temperatures below 10 eV where the mean free path for dissociation can be greater than 1 cm. Under all conditions, the electron temperatures inside the separatrix (see figure 1) are above 10 eV and the $D_\alpha$ radiation following molecular breakup is expected to be small compared to that caused by direct electron excitation. For the H-mode discharges, all the measured temperatures in the divertor are also greater than 10 eV except those adjacent to the floor tiles in the private flux region. However, temperatures in the private flux region of L-mode discharges range from 2 to 30 eV, and significant $D_\alpha$ contributions from dissociative processes several centimetres above the floor tiles in the private flux region cannot be ruled out.

## 3. Computational model

The neutral transport simulations have been carried out with the two-dimensional TEP neutral transport code GTNEUT and with the Monte Carlo code DEGAS. The methodology used in the DEGAS code is documented in [3]. The TEP method and its implementation into the GTNEUT code represent a fast and accurate alternative to Monte Carlo for calculating neutral transport in plasmas.

In this section, we summarize the basic principles of the TEP method and discuss some recent additions and upgrades.

### *3.1. TEP Methodology*

The TEP methodology and its implementation in the GTNEUT code have been published in [4–6]. The TEP methodology

is based on the balance of neutral particle fluxes—or partial currents—at the interfaces of arbitrarily shaped regions into which the domain of interest has been subdivided [4]. The domain of interest usually consists of the edge plasma, extending from well inside the separatrix to the material surfaces forming the plasma chamber. This edge region is partitioned into a number of discrete geometric regions or cells for computational purposes. The total neutral particle flux $\Gamma_{i,j}$ from region $i$ into region $j$, is written as:

$$\Gamma_{i,j} = \sum_k \Gamma_{k,i} T^i_{kj} + \sum_k \Gamma_{k,i}\Big(1 - \sum_l T^i_{kl}\Big) c_i P_i \Lambda_{ij} + S^i_{\text{ext}} P_i \Lambda_{ij} \quad (1)$$

where the first term represents all the fluxes incident on the region $i$ from adjacent regions $k$ which are transmitted across the region $i$ without collisions into region $j$, the second term is the flux due to collided neutrals escaping from region $i$ into region $j$ after having suffered one or more scattering or charge exchange collisions in region $i$, and the last term is due to any volumetric sources of neutrals in region $i$. The first-flight transmission probability $T^i_{kj}$, the scattering/charge exchange fraction of all collisions $c_i$, the total escape probability $P_i$ and the directional probability $\Lambda_{ij}$ have been defined in [4–6] and are not repeated here.

*3.1.1. Reflection Model.* In the original formulation, if region $i$ is bounded by one or more wall segments $kw$, then the boundary condition at this interface is:

$$\Gamma_{kw,i} = R^{kw} \Gamma_{i,kw} + \Gamma^{kw}_{\text{ext}} \quad (2)$$

where $R^{kw}$ is the reflection coefficient of the wall segment $kw$ and $\Gamma^{kw}_{\text{ext}}$ represents any external neutral fluxes (due to gas puffing, etc). In the original GTNEUT code, reflection coefficients were input variables, and the reflected (as well as the externally injected) neutrals were assumed to have energies equal to the ion temperature of the region facing the wall segment from which they were reflected or injected. However, this simple treatment failed to take into account the very different energies associated with the reflected and the re-emitted or gas fuel neutral populations: when ions or neutrals interact with material surfaces, a significant fraction of them are re-emitted as molecules at low energies of the order of the wall temperature which, after dissociation, become Franck–Condon atoms with energies of a few electronvolts [14]. Since all coefficients in equation (1) depend on the neutral energy through their dependence on the neutral mean free path $\lambda$ or on the various ion-neutral reaction rates, neglecting to account for the correct energy distribution can introduce errors in both the uncollided and collided components of neutral fluxes originating from material surfaces.

To treat this problem exactly, the molecules should be transported explicitly until they dissociate, and then the Franck–Condon neutrals should be transported explicitly until they have had one or more charge exchange or elastic scattering collisions and thereby equilibrated with the background ions. In this implementation, we neglect the molecular transport and assume that the molecules are dissociated at the point at which they are introduced into the plasma chamber, but we transport the lower energy Franck–Condon neutrals separately.

The total particle flux from a wall segment $kw$ to an adjacent plasma region $i$, given before by equation (2), is now written as:

$$\Gamma_{kw,i} = \Gamma^{kw}_{\text{ext}} + R^{kw}_n \Gamma_{i,kw} + (1 - R^{kw}_n)(1 - f^{kw}_{\text{abs}})\Gamma_{i,kw} \quad (3)$$

where the first term represents, as before, any external flux contributions, the second term represents the fraction of particles directly reflected or back-scattered while retaining a significant fraction of their original energy, and the last term represents the neutrals that are re-emitted as molecules from the material surface at the wall temperature. In this model, we assume that these molecules dissociate immediately into atoms with the Franck–Condon energy of a few electronvolts.

In equation (3), $R^{kw}_n$ is the particle reflection coefficient, which depends on the impact energy of the ions and the material properties of the surface, and $f^{kw}_{\text{abs}}$ is a wall absorption coefficient taking into account any particles that remain trapped in the wall. To take into account the different energies of these three groups of neutrals that originate from the wall segment $kw$, the various coefficients appearing in equation (1) are now calculated using the correct energy of each group. The externally launched particles (from gas puffing, etc) are assumed to have energy $E_0$ which is treated as an input variable, the back-scattered 'fast' particles have an energy equal to $T_{\text{i}} R^{kw}_{\text{E}}/R^{kw}_n$, where $T_{\text{i}}$ is the ion temperature of the plasma region adjacent to the wall segment $kw$ and $R^{kw}_{\text{E}}$ is the energy reflection coefficient, and the 'slow' neutrals are assumed to emerge at an input-specified low energy corresponding to the Franck–Condon energy for atoms. The particle and energy reflection coefficients $R^{kw}_n$ and $R^{kw}_{\text{E}}$ of each wall segment are calculated using standard fits that are valid for a wide range of wall materials, particle species and impact energies [15, 16].

Using equation (3) to express wall-originated fluxes in terms of plasma region fluxes, as well as using an albedo boundary condition to express the fluxes from the core plasma that is not part of our solution domain [4], equation (1) for an arbitrary region without external sources and bounded by other regions, material walls and core plasma can be written as:

$$\begin{aligned}
\Gamma_{i,j} = {} & \sum_k^{k\neq kw,kpl} \Gamma_{k,i} T^i_{kj} + \sum_k^{k\neq kw,kpl} \Gamma_{k,i}\Big(1 - \sum_l T^i_{kl}\Big) c_{i,k} P_i \Lambda_{ij} \\
& + \sum_{kpl} \alpha_{kpl} \Gamma_{i,kpl} T^i_{kpl,j} \\
& + \sum_{kpl} \alpha_{kpl} \Gamma_{i,kpl}\Big(1 - \sum_l T^i_{kpl,l}\Big) c_{i,kpl} P_i \Lambda_{ij} \\
& + \sum_{kw} \Gamma^{kw}_{\text{ext}} T^{i,0}_{kw,j} + \sum_{kw} R^{kw}_n \Gamma_{i,kw} T^{i,\text{f}}_{kw,j} \\
& + \sum_{kw} (1 - R^{kw}_n)(1 - f^{kw}_{\text{abs}}) \Gamma_{i,kw} T^{i,\text{s}}_{kw,j} \\
& + \sum_{kw} \Gamma^{kw}_{\text{ext}}\Big(1 - \sum_l T^{i,0}_{kw,l}\Big) c^0_{i,kw} P_i \Lambda_{ij} \\
& + \sum_{kw} R^{kw}_n \Gamma_{i,kw}\Big(1 - \sum_l T^{i,\text{f}}_{kw,l}\Big) c^{\text{f}}_{i,kw} P_i \Lambda_{ij} \\
& + \sum_{kw} (1 - R^{kw}_n)(1 - f^{kw}_{\text{abs}}) \Gamma_{i,kw} \\
& \times \Big(1 - \sum_l T^{i,\text{s}}_{kw,l}\Big) c^{\text{s}}_{i,kw} P_i \Lambda_{ij} \quad (4)
\end{aligned}$$

where now the superscripts 0, f, s (for external energy $E_0$, fast and slow energies) appearing in the first-flight transmission probabilities and charge exchange fractions for the wall originated neutrals, and the subscript $k$ appearing in the charge exchange fractions in all other cases, emphasize the fact that these quantities are now calculated at more realistic neutral energies.

*3.1.2. Two-group treatment of slow neutrals.* The implementation of the new reflection model has effectively made the TEP calculation in the regions adjacent to the wall material surfaces, a three-energy group calculation. However, in the inner regions, the calculation still follows the original TEP methodology, which assumes that the neutral energy is equal to the local ion temperature. Extensive tests against Monte Carlo [5, 6] have shown that this 'local ion temperature' model is a reasonable assumption when the neutral mean free path $\lambda$ is comparable to or less than the characteristic dimension $\Delta$ of the region under consideration, and when there are no strong gradients in the background plasma properties. When either of these conditions is not met, however, the possibility of introducing errors in the calculation due to assigning the wrong energy to parts of the neutral population must be considered.

To remedy this situation, the TEP methodology was modified by introducing two distinct energy groups: a 'slow' energy group, consisting of the neutral atoms at the Franck–Condon energy formed by the dissociation of molecules re-emitted from the wall or injected as a gas fuelling source, and a 'fast' energy group including the neutrals that are in thermal equilibrium with the background ion population. Directly reflected neutrals are assumed to be part of the fast group, since they retain a significant fraction of their original energy. Making the plausible simplifying assumption that every charge exchange or elastic scattering reaction moves slow neutrals to the fast neutrals group and that no fast neutrals are 'scattered' from the fast to the slow group, the particle balance equations for the two groups and for internal regions (i.e. regions not bounded by material surfaces) are:

$$\Gamma^{\mathrm{f}}_{i,j} = \sum_k \Gamma^{\mathrm{f}}_{k,i} T^{i,\mathrm{f}}_{k,j} + \sum_k \Gamma^{\mathrm{f}}_{k,i} \Big(1 - \sum_l T^{i,\mathrm{f}}_{k,l}\Big) c_{i,k} P_i \Lambda_{ij} + \sum_k \Gamma^{\mathrm{s}}_{k,i} \Big(1 - \sum_l T^{i,\mathrm{s}}_{k,l}\Big) c^{\mathrm{s}}_i P_i \Lambda_{ij} \tag{5}$$

$$\Gamma^{\mathrm{s}}_{i,j} = \sum_k \Gamma^{\mathrm{s}}_{k,i} T^{i,\mathrm{s}}_{k,j} \tag{6}$$

where the superscripts 's' and 'f' correspond to the slow and fast energy groups. The third term in equation (5) represents the slow neutrals that entered the fast group, after charge-exchanging or scattering with the background plasma ions. From equation (6), we can see that the slow neutrals group propagates only through uncollided fluxes, and does not have any contribution from charge-exchange reactions.

For neutrals originating from wall segments due to reflection, re-emission or external sources, the fast and slow fluxes into the adjacent plasma region are:

$$\begin{aligned} \Gamma^{\mathrm{f}}_{kw,i} &= R^{kw}_n \Gamma^{\mathrm{f}}_{i,kw} \\ \Gamma^{\mathrm{s}}_{kw,i} &= \Gamma^{kw}_{\mathrm{ext}} + (1 - R^{kw}_n)\left(1 - f^{kw}_{\mathrm{abs}}\right)\Gamma^{\mathrm{f}}_{i,kw} \\ &\quad + [R^{kw}_n + (1 - R^{kw}_n)(1 - f^{kw}_{\mathrm{abs}})]\Gamma^{\mathrm{s}}_{i,kw} \end{aligned} \tag{7}$$

It can be seen from equation (7) that only the directly reflected neutrals of the fast energy group are credited to the fast group. The Franck–Condon neutrals resulting from the dissociation of re-emitted or gas fuelling molecules go into the slow group.

## 4. Analysis of DIII-D neutrals experiments

In this section, the results of the GTNEUT simulations of the neutral densities in the two DIII-D discharges described in section 2 are presented and compared to the experimental results, as well as to simulations of these experiments by the Monte Carlo neutral transport code DEGAS.

A more direct comparison between computation and experiment could be carried out by attempting to simulate the TV camera views rather than the neutral densities. This approach would avoid the errors inherent in the inversion of the TV camera data. However, since this version of GTNEUT does not have the capability of producing the necessary quantities for comparison with the raw data, such a direct comparison has not been attempted in this work.

Both GTNEUT and DEGAS use the same two-dimensional geometry and background plasma properties, which were computed with the two-dimensional plasma fluid code B2.5 [17]. The predictions of the B2.5 code for the electron temperature $T_{\mathrm{e}}$ agree well with the divertor Thomson data both inside and outside the separatrix. The corresponding predictions for the electron density $n_{\mathrm{e}}$ underpredict the Thomson scattering data in the private flux region, but otherwise agree well with the experiment inside the separatrix. The latest version of the GTNEUT code can now use the same atomic reaction rate data used in the DEGAS code, so there are no differences between GTNEUT and DEGAS due to the use of different reaction rates. The new reflection model implemented in the GTNEUT code allowed us to run both codes with a consistent treatment of wall reflection, assuming carbon walls.

Since the GTNEUT code cannot handle the transport of molecular species yet, the DEGAS code was run with and without the molecular species option to facilitate the GTNEUT–DEGAS comparison.

### 4.1. L-mode discharge

Here, we compare the predictions of the GTNEUT and DEGAS codes with the experimental neutral measurements for the L-mode DIII-D discharge 96740 at 2250 ms. The geometric model is shown in figure 2. The $X$-point in this discharge was located 13.8 cm above the divertor floor. (The $z$-axis in figure (1) does not correspond to the height over the divertor floor). The shaded cells in figure 2 correspond to the locations at which the neutral density measurements were made.

Typical plasma densities and electron temperatures in the regions just inside the separatrix (61–63 in figure 2) are in the range of (3.2–1.4) $\times 10^{19}$ m$^{-3}$ and 50–75 eV, respectively. Densities and temperatures are considerably lower in the private flux regions. Molecules (used in the 'DEGAS (molecules)' simulations) emerge at a wall temperature of 0.025 eV (300°K) while atomic neutrals (used in GTNEUT and in the DEGAS simulations without molecular transport) are

assumed to have Franck–Condon energies of 3 eV. The neutrals of the gas puffing source are also treated as 3 eV Franck–Condon neutrals. The exact value assumed for the energy of the Franck–Condon neutrals is not very important. To assess the sensitivity of our predictions to the value of this energy, we performed simulations varying the Franck–Condon energy from 1 to 10 eV in both codes. The results of these simulations were very similar, especially for energies below 5 eV.

The results of our GTNEUT and DEGAS simulations, as well as the experimental measurements and their error bars are shown in figure 3, where the various neutral densities are plotted vs the height off the divertor floor. The region to the left of the separatrix line corresponds to the private flux area, and the region to the right is the core plasma. As explained in section 2, the error bars in the private flux region are large due to uncertainties (photon statistics) in the measured Thomson $T_e$ and $n_e$ values and the large sensitivity of the excitation rate coefficients to these uncertainties at low temperatures.

It can be seen from figure 3, that the agreement between GTNEUT and the DEGAS case without molecular transport

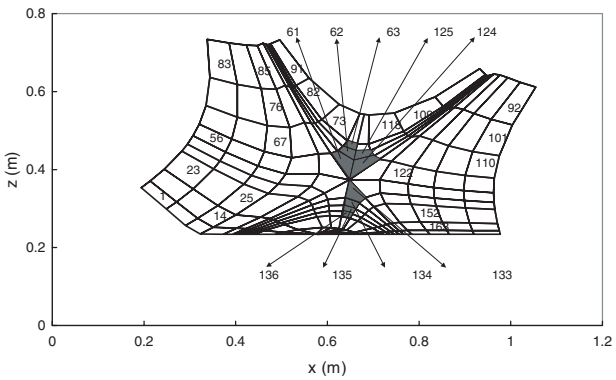


**Figure 2.** Geometry used in the GTNEUT and DEGAS neutral transport simulations of DIII-D L-mode shot 96740 @ 2250 ms. Shaded regions correspond to locations where measurements were made.

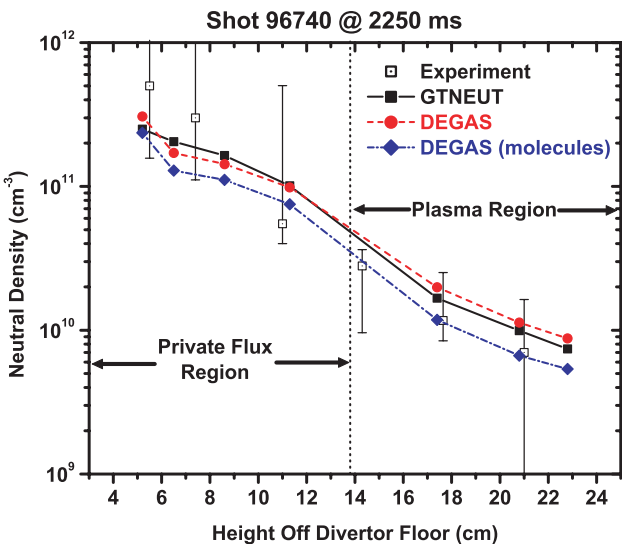


**Figure 3.** Comparison of GTNEUT and DEGAS simulations with experiment for the L-mode DIII-D shot 96740 @ 2250 ms. Atomic neutrals are assumed to have a Franck–Condon energy of 3 eV.

(solid circles) is excellent throughout the entire domain. The predictions of both codes agree with the experiment, being within the error bars of the measurements in all but one case. The DEGAS simulation including molecular transport predicts lower neutral densities compared to GTNEUT and the DEGAS without molecules simulations, and it underpredicts the data in the private flux region. The former is due to the fact that when molecular transport is included, a possible channel for molecular breakup in the DEGAS code is molecular ionization followed by dissociation. The process leaves one neutral atom and one ion, in contrast to the case without molecular transport where all recycled particles are counted as atoms. Both DEGAS simulations (with and without molecules) were carried out using the same gas recycling source. The underprediction of the data in the private flux region in the DEGAS simulation including molecular transport is mainly due to the fact that the experimental analysis also neglected molecular effects. Although this effect is believed to be small overall, it may be non-negligible in the private flux region due to the low electron temperatures there, as explained in section 2.

We previously found [6] good agreement between GTNEUT and DEGAS for this model when the 'mirror' or specular reflection condition was used in DEGAS to match the reflection condition in the earlier version of GTNEUT. However, the new reflection condition in GTNEUT is more realistic and results in much better agreement with experiment than obtained in [6].

### *4.2. H-mode discharge*

In this subsection, the results of our simulations for the H-mode DIII-D discharge 96747 at 3940 ms are presented. The geometric model, which is shown in figure 4, and the plasma properties are identical for the GTNEUT and DEGAS calculations and both codes use the same reaction rate data. The $X$-point in this case was located 10.6 cm above the divertor floor. As before, the shaded cells in figure 4 correspond to the locations at which the neutral density measurements were made. Carbon is assumed as the wall material. As in the L-mode case, molecules are assumed to emerge at the

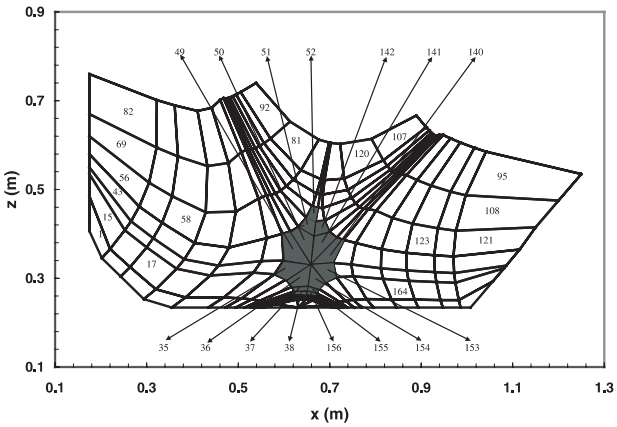


**Figure 4.** Geometry used in the GTNEUT and DEGAS neutral transport simulations of the DIII-D H-mode shot 96747 @ 3940 ms. Shaded regions correspond to locations where measurements were made.

wall temperature of 0.025 eV (corresponding to 300°K), while Franck–Condon neutral atoms are assumed to have energies of 3 eV. Electron temperatures are higher compared to the L-mode experiment both inside and outside the separatrix (100–200 eV in regions 50–52 and 5–40 eV in regions 35–38). Electron densities are also higher compared to the L-mode.

The results of our GTNEUT and DEGAS simulations are shown in figure 5, where the calculated and measured neutral densities, including the experimental error bars, are plotted vs the height off the divertor floor. As before, DEGAS was run with and without molecular transport. It can be seen from figure 5 that the agreement between GTNEUT and DEGAS without molecular transport is good, while DEGAS with molecular transport predicts lower neutral densities. The GTNEUT predictions are within the error bars of the experimental measurements with the exception of the last three points inside the plasma core, where GTNEUT overpredicts the experiment. DEGAS without molecular transport slightly underpredicts the experiment in the private flux region, while DEGAS with molecular transport underpredicts the experiment in the private flux region, but is closer to the data well inside the plasma core. It should be noted that the apparent better agreement of the GTNEUT predictions with the data shown in figure 5 is probably fortuitous and should not be interpreted as evidence of any implied superiority of the TEP method vs Monte Carlo. As in the L-mode case, the underprediction of the data by the DEGAS simulation with molecular transport in the private flux region can be attributed to the fact that the experimental analysis also neglected molecular effects.

As in the L-mode case, the lower neutral densities predicted by the DEGAS with molecular transport simulation can be attributed to the possibility of molecular ionization followed by dissociation, which decreases the net atom source. Analysis of molecular transport in DIII-D experiments will be revisited after GTNEUT is upgraded with molecular transport capability and using the more recent DEGAS-2 code which has better atomic and molecular reaction data [18].

As mentioned in the beginning of this section, both GTNEUT and DEGAS use the background plasma predicted by the B2.5 code. The electron density predictions of the B2.5 code underpredict the Thomson scattering data in the private flux region, but otherwise agree well with the experiment inside the separatrix. To see whether this density underprediction in the private flux region could explain the overprediction of neutral penetration by both simulations in the plasma region, GTNEUT was run by increasing the electron densities in the private flux region. The results show that a factor of two enhancement of the electron density in the private flux region results in a corresponding decrease of the neutral density by about 15% in the private flux region, while the neutral densities inside the plasma are mostly unaffected. This effect is too small to affect the comparison of the simulations with the experiment.

Finally, in order to illustrate the effect of the 2-group energy approach implemented in GTNEUT and described in the previous section, the predictions of the original, single-group, GTNEUT code are compared with the 2-group GTNEUT and the experiment in figure 6. The improvement due to the 2-group calculation is apparent both inside and outside the separatrix.

The large discrepancy between the 1-group and 2-group GTNEUT predictions, can be explained as follows: the mean free path of the slow neutrals in the H-mode case was several times larger than the typical dimension of the cells ($\lambda/\Delta \sim 3$–5) near the region of interest in the private flux area between the $X$-point and the bottom of the divertor floor. As a result, low energy Franck–Condon neutrals that were transported uncollided into inner plasma regions were treated in the original, single energy group, version of the GTNEUT code as having energies equal to the much higher local ion temperatures. This overestimation of the average neutral energy near the regions of interest led to an underestimation of the overall neutral densities in these regions.

The differences between the 1-group and 2-group GTNEUT predictions are much smaller in the L-mode case. The reason for this is that the background plasma temperatures in the L-mode case were much lower compared to the H-mode

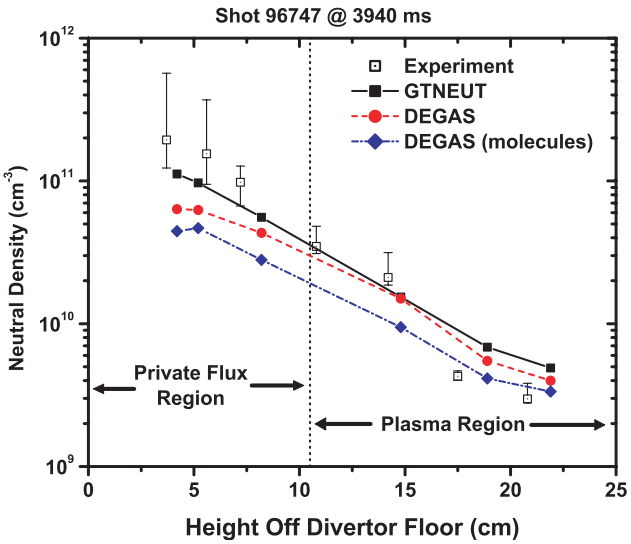


**Figure 5.** Comparison of GTNEUT and DEGAS simulations with experiment for the DIII-D H-mode shot 96747 @ 3940 ms. Atomic neutrals are assumed to have a Franck–Condon energy of 3 eV.

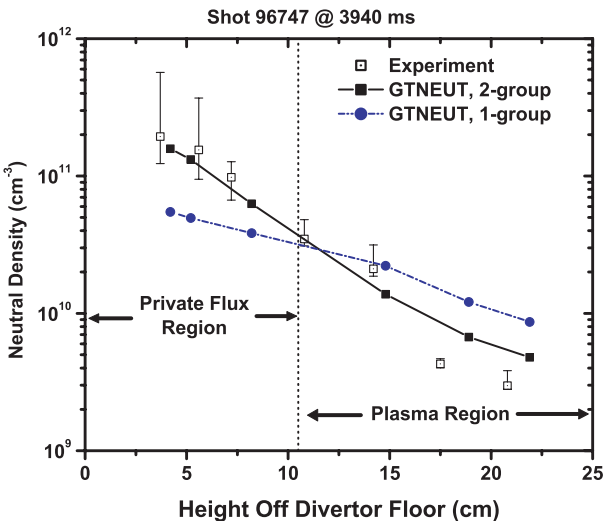


**Figure 6.** Comparison of the predictions of the 2-group and the original 1-group GTNEUT with the experimental data for the DIII-D H-mode shot 96747 @ 3940 ms.

case, so treating all neutrals as belonging to the same energy group (at thermal equilibrium with the background ions) did not introduce a significant error.

## 5. Conclusions

Simulations with the GTNEUT (TEP method) and DEGAS (Monte Carlo method) codes of the neutral densities in two recent DIII-D discharges (L-mode and H-mode) are in good agreement with measured values.

The implementation of several new and improved models in the GTNEUT code, including a wall reflection model, a two energy group formulation and the capability to use in GTNEUT the atomic reaction rate data from the DEGAS code, has resulted in quite good agreement between the predictions of the two codes.

## Acknowledgments

This work was supported by the US Department of Energy under Grant No DE-FG02-99-ER54538 with the Georgia Tech Research Corporation and under Contract Nos DE-ACO5-96OR22464 with the Oak Ridge National Laboratory and DE-AC03-99ER54463 with General Atomics.

## References

[1] Colchin R.J. *et al* 2000 *Nucl. Fusion* **40** 175
[2] Fenstermacher M.E. *et al* 1997 *Rev. Sci. Instrum.* **68** 974
[3] Heifetz D. *et al* 1982 *J. Comput. Phys.* **46** 309
[4] Stacey W.M. and Mandrekas J. 1994 *Nucl. Fusion* **34** 1385
[5] Stacey W.M., Mandrekas J. and Rubilar R. 2001 *Fusion Sci. Technol.* **40** 66
[6] Rubilar R., Stacey W.M. and Mandrekas J. 2001 *Nucl. Fusion* **41** 1003
[7] Stacey W.M. 2000 *Nucl. Fusion* **40** 965
[8] Janev R.K. *et al* 1987 *Elementary Processes in Hydrogen-Helium Plasmas* (Berlin: Springer)
[9] Fielding S.J. *et al* 1989 *J. Nucl. Mater.* **162–164** 482
[10] Janev R.K. and Smith J.J. 1993 *Atomic and Plasma Material Interaction Data for Fusion* (Suppl. to *Nucl. Fusion)* vol 4 (Vienna: IAEA) p 1
[11] Isler R.C. 2002 Oak Ridge National Laboratory, USA, Private communication
[12] Fenstermacher M.E. *et al* 1997 *Phys. Plasmas* **4** 1761
[13] Nilson D.G. *et al* 1997 *Fusion Eng. Des.* **34–35** 609
[14] Stangeby P.C. 2000 *The Plasma Boundary of Magnetic Fusion Devices* (Philadelphia: Institute of Physics Publishing)
[15] Thomas E.W., Janev R.K. and Smith J. 1992 *Nucl. Instrum. Methods* B **69** 427
[16] Eckstein W. 1997 *J. Nucl. Mater.* **248** 1
[17] Braams B.J. 1996 *Contrib. Plasma Phys.* **36** 276
[18] Stotler D.P. and Karney C.F.F. 1994 *Contrib. Plasma Phys.* **34** 392